

A Divergence-free Meshless Method for Transient Vector Wave Equations

Shunchuan Yang¹, Donglin Su¹, and Zhizhang (David) Chen²

¹School of Electronic and Information Engineering
Beihang University, Beijing, 100083, China
scyang@buaa.edu.cn

²Department of Electrical and Computer Engineering
Dalhousie University, Halifax, Nova Scotia, B3H 4R2, Canada

Abstract — With the implementation of the vector radial basis function (RBF), which is theoretically divergence free, we propose a meshless method for solving the transient vector wave equation. Unlike the conventional radial point interpolation meshless (RPIM) method based on the scalar RBF that solves electric field and magnetic field components separately with scalar wave equations, the proposed method solves the vector wave equation directly. Therefore, the long-existing technical challenge of the source in the traditional RPIM method is resolved due to the direct solution of the vector wave equation. In addition, the stability condition of the proposed method is presented. At last, several numerical experiments are conducted to validate the accuracy of the proposed solver.

Index Terms — Divergence free, meshless, RPIM, vector radial basis function (RBF).

I. INTRODUCTION

Compared with the conventional numerical methods such as the finite-difference time-domain (FDTD) method, the method of moment (MOM) and the finite-element (FEM), the meshless methods have various intrinsic merits of conformal modeling, multi-scale adaptation and relatively easy node refinement. With these merits, many efforts have been made to develop various forms of the node-based meshless methods in the recent years. They include the element-free Galerkin method [1], the moving least square reproducing kernel method [2], the smoothed particle electromagnetic method [3], the radial point interpolation meshless (RPIM) method [4], the 3-D RPIM method [5] and its unconditional stable version [6]. In these meshless methods, only spatial node location information is needed to model electromagnetic problems. No connection information among nodes is required, which is the main difference between spatial nodes and discrete mesh. As a result, the re-arrangement of grid lines is no longer

required when a structure is modified and refined partially.

Another issue associated with the numerical methods, especially the time-domain based numerical solvers, is the divergence property: in a continuous domain, magnetic fields are always divergence-free and so are electric fields in charge free regions. When we develop numerical methods for solving electromagnetic problems, this divergence property may or may not be preserved. Somehow this issue has been ignored in most literatures. If the divergence property is not preserved, spurious numerical solutions may emerge and lead to incorrect results [7]. Indeed, it has been found that the conventional radial point interpolation meshless (RPIM) method does not always retain this divergence-free property and spurious solutions do show up in the solutions [8].

Towards this end, the divergence-free vector-based RBFs were developed for non-electromagnetic or non-electrical applications. A matrix-valued vector RBF, which is different from the scalar RBF, was developed and proven theoretically divergence free [9]. More work was presented in [9-13]. In particular, the divergence-free vector RBF was successfully developed for Navier-Stokes equation [11,12] and astrophysical magneto-hydrodynamics (MHD) [13]. We successfully applied vector RBFs to solve Maxwell's equations with detailed discussion of the properties of the vector RBFs [14]. However, like the conventional RPIM method where all six field components are solved, the method presented in [14] still requires dual sets of the nodes (E- and H-nodes). This increases computational cost compared with other methods directly solving the wave equations.

In this paper, we propose a meshless method which is incorporated with the vector RBF for solving the full vector wave equations. We have reported our initial results in [15]. In the proposed method, only one set of field quantities (either E- or H-fields) needs to be dealt with. Therefore, it is easier to implement than the method

proposed in [14]. Since we solve the vector wave equation like the vector FEM, only \mathbf{E} or \mathbf{H} fields are available. For most applications, it is enough to extract the interested parameters. However, if we indeed need to another type fields, it could be quite easy to obtain through the Maxwell's equations without any troubles.

The paper is organized in the following manner. In Section II, detailed formulations of the proposed meshless method for the solutions of vector wave equation are described. In Section III, the stability condition of the proposed method is presented. In Section IV, accuracy of the proposed method is verified with numerical examples. Finally, the conclusion is drawn in Section V.

II. THEORY

Without losing the generality, we consider the general second-order vector wave equation for the electrical field in a lossless medium:

$$\nabla \times \frac{1}{\mu_r} \nabla \times \mathbf{E}(\mathbf{r}, t) + \frac{\varepsilon_r}{c_0^2} \partial_t^2 \mathbf{E}(\mathbf{r}, t) = -\mu_0 \partial_t \mathbf{J}(\mathbf{r}, t), \quad (1)$$

where $\mathbf{E}(\mathbf{r}, t)$ is the electric field, $\mathbf{J}(\mathbf{r}, t)$ is the current density, ε is permittivity of the medium, μ_0 is the permeability of the free space, μ_r is the relative permeability of the medium.

To obtain the numerical solution of (1), a solution domain is first discretized with spatial nodes pre-defined by users. Then electric field $\mathbf{E}(\mathbf{r}, t)$ is approximated in expansion with the following node-based vector shape functions:

$$\mathbf{E} = \sum_i^N \Phi_i \mathbf{E}_i, \quad (2)$$

where N is the number of the scattering nodes in the local support domain, Φ_i is the vector shape function associated with the node i with dimension of 3×3 , \mathbf{E}_i is the corresponding expansion coefficient in vector (field vector) with respect to node i and it is of the dimension of 3×1 . By using (2) to approximate the electric field, we need to properly define the vector shape functions that embody the divergence-free property mentioned before.

Mathematically, a divergence free field, denoted as \mathbf{u} , can always be expressed as the curl of another vector field with the definition of Coulomb gauge [11,12]:

$$\begin{aligned} \mathbf{u} &= \nabla \times \nabla \times \sum_{j=1}^N \phi(\mathbf{R} - \mathbf{R}_j) \mathbf{A}_j \\ &= (-\Delta \mathbf{I} + \nabla \nabla^T) \sum_{j=1}^N \phi(\mathbf{R} - \mathbf{R}_j) \mathbf{A}_j \end{aligned}, \quad (3)$$

where $\nabla = \left[\frac{\partial}{\partial x}, \frac{\partial}{\partial y}, \frac{\partial}{\partial z} \right]^T$, ϕ is a preselected scalar basis function, $\mathbf{A}_j = (A_{xj}, A_{yj}, A_{zj})^T$ is the unknown vector

expansion coefficient to be determined, \mathbf{I} is 3×3 identity matrix and Δ is the Laplace operator, which can be expressed as:

$$\Delta = \begin{bmatrix} \frac{\partial^2}{\partial x^2} + \frac{\partial^2}{\partial y^2} + \frac{\partial^2}{\partial z^2} & & \\ & \frac{\partial^2}{\partial x^2} + \frac{\partial^2}{\partial y^2} + \frac{\partial^2}{\partial z^2} & \\ & & \frac{\partial^2}{\partial x^2} + \frac{\partial^2}{\partial y^2} + \frac{\partial^2}{\partial z^2} \end{bmatrix}. \quad (4)$$

The scalar Gaussian radial basis function (RBF) is selected as the scalar basis function in this paper which is expressed as $\phi_j = e^{-\alpha|\mathbf{r}-\mathbf{r}_j|^2} = e^{-\alpha r^2}$, $\mathbf{r} = (x, y, z)$ is the position vector of the observation point, $\mathbf{r}_j = (x_j, y_j, z_j)$ is the position vector of node j , $r = |\mathbf{r} - \mathbf{r}_j|$ is the distance between observation node \mathbf{r} and node \mathbf{r}_j , and α is called the shape parameter which controls the decaying rate of the RBF.

By substituting $\phi_j = e^{-\alpha|\mathbf{r}-\mathbf{r}_j|^2} = e^{-\alpha r^2}$ into (3), we can find the vector RBF Ψ_j related to node j , which is defined on node j , and shape function Φ as:

$$\Psi_j = (-\Delta \mathbf{I} + \nabla \nabla^T) \phi_j, \quad (5a)$$

$$\Phi_j = \mathbf{B}_v \mathbf{A}_v^{-1} \mathbf{u}_s, \quad (5b)$$

and

$$\mathbf{u} = \sum_{j=1}^N \Phi_j \mathbf{u}_j, \quad (5c)$$

where

$$\mathbf{u}_s = [\dots \ u_{jx} \ u_{jy} \ u_{jz} \ \dots]^T, \quad \mathbf{u}_j = [u_{jx} \ u_{jy} \ u_{jz}]^T,$$

\mathbf{B}_v includes the vector RBFs, which could be expressed as:

$$\mathbf{B}_v = [\Psi(\|\mathbf{R}_1 - \mathbf{R}_1\|) \ \Psi(\|\mathbf{R}_1 - \mathbf{R}_2\|) \ \dots \ \Psi(\|\mathbf{R}_1 - \mathbf{R}_n\|)],$$

and

$$\mathbf{A}_v = \begin{bmatrix} \Psi(\|\mathbf{R}_1 - \mathbf{R}_1\|) & \Psi(\|\mathbf{R}_1 - \mathbf{R}_2\|) & \dots & \Psi(\|\mathbf{R}_1 - \mathbf{R}_n\|) \\ \Psi(\|\mathbf{R}_2 - \mathbf{R}_1\|) & \Psi(\|\mathbf{R}_2 - \mathbf{R}_2\|) & \dots & \Psi(\|\mathbf{R}_2 - \mathbf{R}_n\|) \\ \vdots & \vdots & \ddots & \vdots \\ \Psi(\|\mathbf{R}_n - \mathbf{R}_1\|) & \Psi(\|\mathbf{R}_n - \mathbf{R}_2\|) & \dots & \Psi(\|\mathbf{R}_n - \mathbf{R}_n\|) \end{bmatrix}.$$

The dimension of \mathbf{A}_v is $3N \times 3N$ and \mathbf{B}_v $3 \times 3N$. The dimension of the interpolation matrix for the conventional RPIM method is $N \times N$. Therefore, the time- and memory-consumption for the construction of the vector shape function are larger than that with the conventional RPIM method for a single node. Since local RBF is usually selected so that N is relatively small. Therefore, the computational cost to construct the shape function from (5b) is relatively small compared with that of overall simulation time. In addition, only one set of electric

nodes needs to be solved and the computational efficiency of the proposed method remains reasonably high.

After expanding the (5a), we obtain the vector RBFs in terms of the scalar RBFs in reference to node j :

$$\Psi_j = \begin{bmatrix} -\partial_y^2 - \partial_z^2 & \partial_x \partial_y & \partial_x \partial_z \\ \partial_y \partial_x & -\partial_x^2 - \partial_z^2 & \partial_y \partial_z \\ \partial_z \partial_x & \partial_z \partial_y & -\partial_x^2 - \partial_y^2 \end{bmatrix} \phi_j. \quad (6)$$

The detailed properties of the vector RBF and theoretical proof of their divergence properties can be found in [11]. To better understand the vector RBFs, a two dimensional vector RBF at $\mathbf{r}_j = [0 \ 0]^T$ with $\alpha = 5$ [13] is plotted in two dimension in Fig. 1. It is easy to find that the first two rows of the vector RBF present two mutually orthogonal dipole modes: Fig. 1 (a) is the horizontal dipole mode and Fig. 1 (b) is the vertical dipole mode; rotation of one dipole leads to another. Obviously, both dipole modes are divergence free. Therefore, the field expanded by them is divergence free.

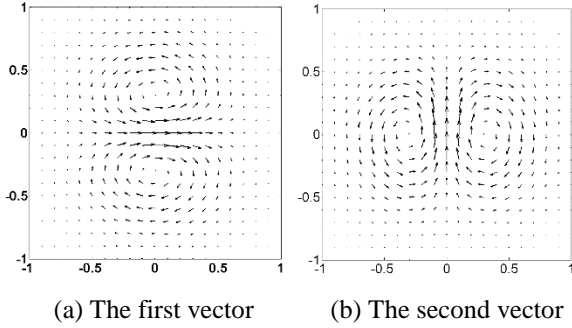


Fig. 1. Vector RBF visualization with $\alpha=5$.

Because of the vector nature of the proposed shape function, the curl operation upon the expanded fields can easily be obtained after applying the curl operator to the vector shape function. Then, we have the following results:

$$\nabla \times \Psi_j = \begin{bmatrix} 0 & -\partial_x^2 \partial_z - \partial_z^3 - \partial_y^2 \partial_z & \partial_x^2 \partial_y + \partial_y^3 + \partial_z^2 \partial_y \\ \partial_x^2 \partial_z + \partial_z^3 + \partial_y^2 \partial_z & 0 & -\partial_z^2 \partial_x - \partial_x^3 - \partial_y^2 \partial_x \\ -\partial_x^2 \partial_y - \partial_y^3 - \partial_z^2 \partial_y & \partial_z^2 \partial_x + \partial_x^3 + \partial_y^2 \partial_x & 0 \end{bmatrix} \phi_j, \quad (7a)$$

$$\nabla \times \nabla \times \Psi_j = (\partial_x^2 + \partial_z^2 + \partial_y^2) \begin{bmatrix} \partial_y^2 + \partial_z^2 & -\partial_x \partial_y & -\partial_x \partial_z \\ -\partial_x \partial_y & \partial_x^2 + \partial_z^2 & -\partial_z \partial_y \\ -\partial_x \partial_z & -\partial_z \partial_y & \partial_x^2 + \partial_y^2 \end{bmatrix} \phi_j, \quad (7b)$$

When the variables in the z direction remain constant, (7) reduce to the two-dimensional cases and it is significantly simplified. We obtain the following formulations:

$$\nabla \times \Psi_j = \begin{bmatrix} 0 & 0 & \partial_x^2 \partial_y + \partial_y^3 \\ 0 & 0 & -\partial_x^3 - \partial_y^2 \partial_x \\ -\partial_x^2 \partial_y - \partial_y^3 & \partial_x^3 + \partial_y^2 \partial_x & 0 \end{bmatrix} \phi_j, \quad (8a)$$

$$\nabla \times \nabla \times \Psi_j = (\partial_x^2 + \partial_y^2) \begin{bmatrix} \partial_y^2 & -\partial_x \partial_y & 0 \\ -\partial_x \partial_y & \partial_x^2 & 0 \\ 0 & 0 & \partial_x^2 + \partial_y^2 \end{bmatrix} \phi_j. \quad (8b)$$

With the well-defined vector shape function and spatial placement of the nodes in the solution domain, we can solve the vector wave equation (1) with the proposed vector-based meshless method. By substituting (2) into (1), we get the semi-discretized vector wave equation:

$$\nabla \times \frac{1}{\mu_r} \nabla \times \sum_i^N \Phi_i \mathbf{E}_i + \frac{\epsilon_r}{c_0^2} \partial_t^2 \sum_i^N \Phi_i \mathbf{E}_i = -\mu_0 \partial_t \mathbf{J}. \quad (9)$$

To make (9) practical for computation, the collocation approach is applied to (9), which means that we test (9) with Dirac Delta function associated centered at node i . Due to the Kronecker's delta property of the shape function [14], we obtain the semi-discretized formulation:

$$\left(\nabla \times \frac{1}{\mu_r} \nabla \times \sum_j^N \Phi_j \mathbf{E}_j \right) \Big|_{node_i} + \frac{\epsilon_r}{c_0^2} \partial_t^2 \mathbf{E}_i = -\mu_0 \partial_t \mathbf{J} \Big|_{node_i}. \quad (10)$$

By applying the central finite difference in the time domain to (9), we reach the final time-marching formulation:

$$\mathbf{E}_i^{n+1} = 2\mathbf{E}_i^n - \mathbf{E}_i^{n-1} - \frac{c_0^2 \Delta t^2}{\epsilon_r} \left(\nabla \times \frac{1}{\mu_r} \nabla \times \sum_j^N \Phi_j \mathbf{E}_j^n \right) \Big|_{node_i} - \frac{\Delta t^2}{\epsilon} \partial_t \mathbf{J} \Big|_{node_i}. \quad (11)$$

To make (11) more compact, we split and compute (11) in two steps:

$$\mathbf{Q}_i^{n+1} = \mathbf{Q}_i^n - \frac{\Delta t^2}{\mu_0 \epsilon} \left(\nabla \times \frac{1}{\mu_r} \nabla \times \sum_j^N \Phi_j \mathbf{E}_j^n \right) \Big|_{node_i} - \frac{\Delta t^2}{\epsilon} \partial_t \mathbf{J} \Big|_{node_i}, \quad (12a)$$

$$\mathbf{E}_i^{n+1} = \mathbf{Q}_i^{n+1} + \mathbf{E}_i^n, \quad (12b)$$

where \mathbf{Q} is the intermediate vector introduced to speed up the computation. (11) is a vector form that can be directly solved without the need to expand the Maxwell's equations into six scalar partial derivative equations for six field components (unlike what is done with the conventional methods).

With the conventional RPIM method and the FDTD method, the vector field equations are expanded into separate scalar wave equations and numerical methods are adopted and applied to solve each of the scalar equations, respectively; this poses a technical challenge when the current source or charges are encountered: field components need to be coupled and computed with nonzero divergence at source points or charge locations. However, now with the proposed meshless method based on the divergence-free vector RBFs, the issue no longer exists since a source term is incorporated into (11) and the wave equations are solved in a coupled vector manner.

When compared with the conventional time-domain

finite-element method, the proposed meshless method is a node-based solver where only the spatial locations of the nodes that discretize the solution domain need to be known; in other words, the node-based property of the meshless methods is preserved including its capability of conforming and multiscale modeling.

III. STABILITY CONDITION

Since the proposed meshless method deploys explicit time-marching scheme, it is conditionally stable. We can obtain its stability condition based on the result presented in [16] for the proposed vector meshless method,

$$\Delta t \leq \frac{\sqrt{|\lambda|_{\max}}}{c_0 \sqrt{\rho(\mathbf{T})}}, \quad (13)$$

where λ is the eigenvalue of matrix $-\frac{\Delta t^2}{\mu_0 \epsilon} \mathbf{T}$, $\rho(\mathbf{T})$

is the spectral radius of \mathbf{T} whose element is $T_{ij} = \left(\nabla \times \frac{1}{\mu_r} \nabla \times \sum_j^N \Phi_j \right) \Big|_{node_i}$. We could find that T_{ij}

is a function of the vector RBF corresponding to the corresponding node and material parameters, more specific, relative permeability. Therefore, the node location and material information are embodied into \mathbf{T} . For homogeneous media, $|\lambda|_{\max} = 4$ can be obtained. Therefore, all temporal steps in the proposed meshless method should satisfy the following condition:

$$\Delta t \leq \frac{2\epsilon_r}{c_0 \sqrt{\rho(\mathbf{T})}}. \quad (14)$$

To determine the maximum time step allowed in the proposed method, we need to evaluate the eigenvalues of \mathbf{T} . As stated in [5], those eigenvalues are related to the minimum node space. When a large number of nodes are involved, direct evaluation of (14) is quite time-consuming and another solution is to select an approximated time step through minimum nodal spacing in [5].

IV. NUMERICAL RESULTS

In this section, we choose several numerical experiments to validate the accuracy and convergence properties of the proposed meshless method for the vector wave equations.

A. One dimensional structure

Due to the existence of the analytical solutions of the one-dimensional cavity with perfect electric conductor

(PEC), we select it for the initial verification of the proposed method. The length of the cavity is 1 meter. The initial condition of the electric field is given as $E_z = \sin(k\pi x/L)$ and the region is source free. The theoretical field distribution is given as:

$$E_z = \cos(k\pi ct/L) \cdot \sin(k\pi x/L), \quad (15)$$

where k is the mode number and L is the length of the cavity.

The nodes are selected uniformly distributed in the cavity with the distance between two neighboring nodes being 1 mm. The shape parameter is selected as 10 and the average node number in each local support domain is 7. For fair comparison, the cavity was also simulated with the FDTD with the uniform of cell size of 1mm, which implies that two method have the same number of field points. To reduce the effect of the time step on the accuracy, the time steps for the proposed meshless method and the FDTD method are selected small so that CFLN = 0.1, where CFLN is the ratio of the time step to the maximum time step allowable with the FDTD method and similar definition in two and three dimensional cases.

Figure 2 shows the field value obtained with the FDTD method and the proposed solver at 10 ns. Good agreements between the results obtained with the proposed method, the FDTD method and the analytical solution are observed. However, we can find that at the peak the proposed method can achieve more accurate solution than that of the FDTD method. Figure 3 presents the absolute error between the numerical solutions and the analytical results. At the peak the error of the proposed method is three times smaller than that of the FDTD method. It confirms that the proposed solver can obtain more accurate results than those of the FDTD method.

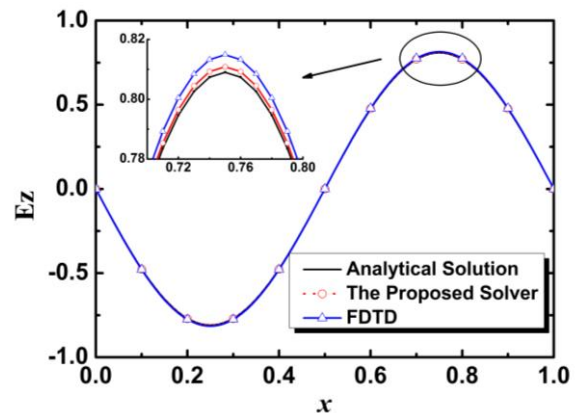


Fig. 2. The E_z field value at 10 ns.

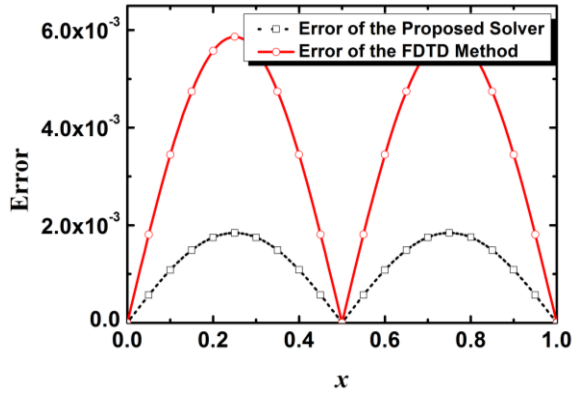


Fig. 3. The absolute solution difference between the proposed method and the FDTD method.

Figure 4 illustrates the relative L_2 error; the L_2 error is computed with the equation below:

$$L_2 = \log_{10} \left(\frac{\|\mathbf{E}^N - \mathbf{E}^A\|_2}{\|\mathbf{E}^A\|_2} \right), \quad (16)$$

where \mathbf{E}^N is the numerical electrical field obtained with the FDTD method or the proposed method and \mathbf{E}^A is the analytical field solution. The error of the two methods goes up as k increases. This is because that the dispersion errors increase with the mode number when the spatial discretization remains unchanged. However, the accuracy of the proposed method is about two order higher than that of the FDTD method. The reason is that the meshless method is essentially a high order method and more nodes are involved in the support domain than that of the FDTD method for each time step updating.

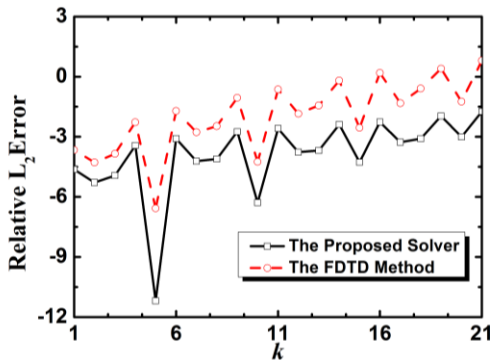


Fig. 4. The relative L_2 error of the proposed solver and the FDTD method.

B. Two-dimensional structure

We also considered an air-filled perfect electric conducting (PEC) cavity with PEC boundary conditions. The cavity is a good structure for numerical validation since it embodies multiple incidences and reflections of

electromagnetic waves. The dimensions of the cavity under consideration are $1 \text{ m} \times 1 \text{ m}$ with uniform discretization of cell size 2 cm. The initial condition is given as:

$$E_z = \sin(m\pi x)\sin(n\pi y), \quad (17)$$

where m and n are the mode numbers in the x and y directions, respectively. The theoretical electric field inside the cavity can be expressed as:

$$E_z = \sin(m\pi x)\sin(n\pi y)\cos(\omega t), \quad (18)$$

where $\omega = c_0\pi\sqrt{m^2 + n^2}$.

A small time step, CFLN=0.1, is selected again for the FDTD method and the proposed method to decrease the numerical error. The average number of the nodes considered in the local support domain is 9 and the shape parameter is selected to be 5 for Gaussian radial basis function (RBF). The distance between two nearest nodes is 0.02 m. The cell size is also 0.02m for the FDTD method. Therefore, the spatial resolutions for the proposed method and the FDTD are the same to make fair comparison.

Figure 5 shows E_z field obtained with the proposed method at 10 ns with $m = 2$, and $n = 2$ for TM_{22} . Figure 6 presents the absolute error of the results obtained with the two methods at 10 ns. The error pattern distribution of the proposed method is the same as that of the FDTD method. However, the magnitudes are smaller than those of the FDTD method. It means that the proposed method can obtain more accurate results than the FDTD method. Again, this is because the proposed meshless method is essentially a higher-order method.

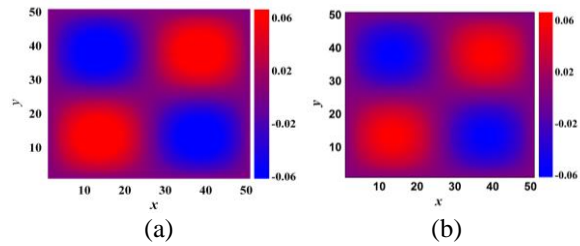


Fig. 5. The analytical field (a) and numerical value obtained from the method (b) at 10 ns.

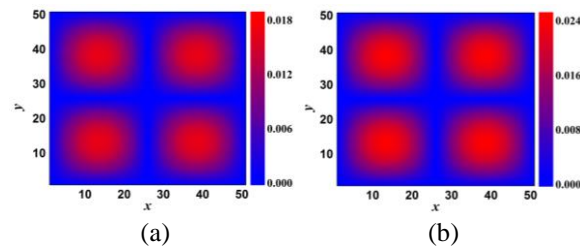


Fig. 6. The absolute error for the proposed method (a) and the FDTD method (b) at 10 ns.

Figure 7 illustrates the relative L_2 error changing with m with fixed n . It can be found that the errors of the proposed method are smaller than those of the FDTD method for all the m modes with $n = 1$ and $n = 3$. Another interesting observation is that as m increases, the L_2 errors of the two methods level off to the same value. This is because the spatial sampling density is not sufficient to capture highly-varied field distributions of the higher modes with large m and n .

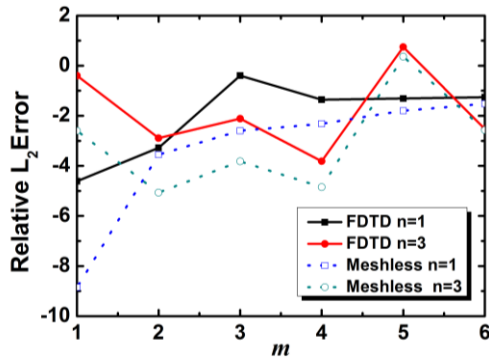


Fig. 7. The L_2 error of the proposed method and the FDTD method verse m with $n=1$ and $n=3$ at 10 ns.

C. Three-dimensional structure

In a three-dimensional case, an air-filled PEC cavity with PEC boundary condition and dimensions of $1\text{ m} \times 1\text{ m} \times 1\text{ m}$ is considered. Again the cavity is a good structure for numerical validation since it embodies multiple incidences and reflections of electromagnetic waves. The cavity is discretized with uniform discretization of cell size 0.1 m. When the same initial condition for the two-dimensional case is chosen, the exactly same analytical solution is obtained. We choose a quite small time step (CFLN=0.1) for the FDTD method and the proposed method to decrease the numerical error. Average number of the nodes in the local support domain is 16 and the shape parameter is 0.5. The distance between two nearest nodes is 0.1 m. The cell size is also 0.1m for the FDTD method to make fair comparison.

Figure 8 presents E_z field obtained from the proposed solver at 10.5 ns with $m = 2$, and $n = 2$. The field distribution is TM_{22} mode. As shown in Fig. 9, the error pattern of the proposed method is exactly the same as that of the FDTD method. However, its magnitudes are smaller than those of the FDTD method, which means that the proposed method can obtain more accurate results than the FDTD method. Again, the reason is that the proposed meshless method is a high order method.

Figure 10 presents the relative L_2 error changing with m . It can be found that the error of the proposed method is smaller than that of the FDTD method for all the m modes with $n = 1$ and $n = 2$. The relative L_2 errors

of the two methods increase as m goes up. To obtain more accurate results for higher-order modes, denser nodes are required for the two methods. Another interesting observation is that for the FDTD method, the error of TM_{11} is larger than that of TM_{12} at 10.5 ns; so is for the proposed method.

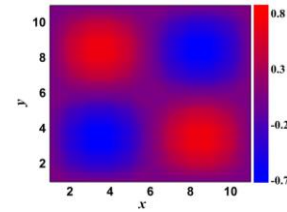


Fig. 8. The field value obtained from the proposed method at 10.5 ns.

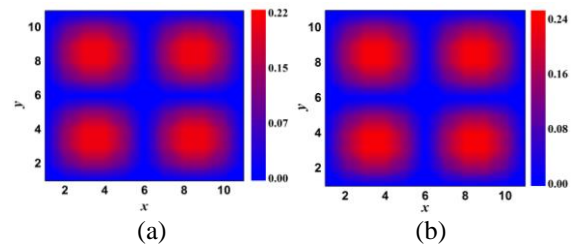


Fig. 9. The absolute error for the proposed method (a) and the FDTD method (b) at 10.5 ns.

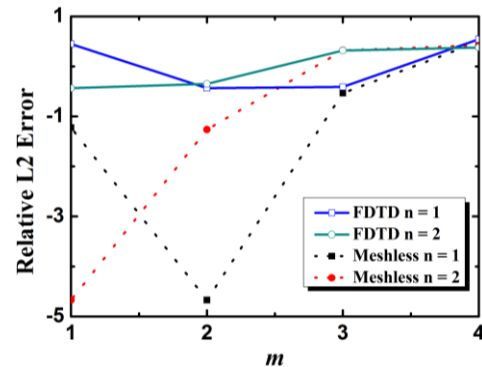


Fig. 10. The L_2 error of the proposed solver and the FDTD method verse m with $n=1$ and $n=2$ at 10.5 ns.

Figure 11 shows the charge density in dB, at $z = 0.4\text{ m}$, obtained from the proposed method with $m = 2$ and $n = 2$ at 10.5 ns. The charge density level is about -15 dB which is at the level of numerical noise. In other words, we can safely consider no artificial charge accumulation for the proposed method like other divergence-free methods, such as the FDTD method.

The FDTD method takes 0.42 s and 5 Mb memory to complete the simulation, however, the proposed method, takes 1.18 s and 5 Mb memory. This is because

in the proposed method more nodes are involved for field updating. However, it could be mitigated to further explore the conformal modelling and coefficient reuse when regular node distribution is used. We will explore those possibilities in the future.

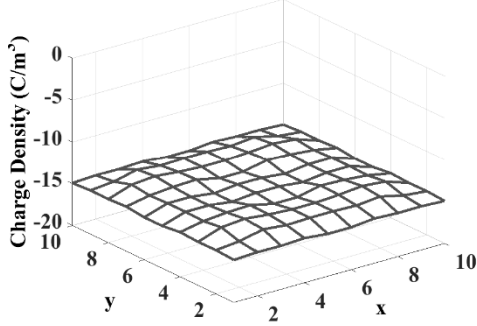


Fig. 11. The charge density at $z = 0.4$ m plane of the proposed solver with $n=2$ and $m=2$ at 10.5 ns. Note: charge density is in dB scale.

Some further remarks upon the proposed vector meshless method are made here: (a) as we have shown in the numerical experiments, the proposed method show the promising potential to serve as a general numerical method, like the FDTD method, but with more accurate results with the same level of discretization. (b) When certain applications, such as electron emission [17], in which the divergence properties are of significant importance are considered, the proposed method could be a better option than the traditional RPIM [5]; since the proposed method is divergence-preserved without introducing any artificial charges. (c) Another issue is how to define a good node distribution in the computational domain. Some early researches have been done in [18]. Interested readers are referred to them for more details.

Currently, we are working on development of the perfectly matched layer so that the proposed method could solve practical complex problems.

V. CONCLUSION

A vector-based meshless method is proposed for the transient electromagnetic analysis. The proposed method is based on the vector RBF and is proven to be divergence free. It solves the vector wave equation directly rather than the corresponding scalar wave equations separately. Therefore, only one set of field quantities (either E- or H-fields) needs to be solved. Its numerical accuracy and convergence properties are investigated through numerical experiments and compared with the analytical solutions. The numerical results reveal that the proposed method offers higher numerical accuracy than the FDTD method with the same level of discretization density.

VI. APPENDIX

The fourth order partial derivative of the Gausses RBF is expressed as:

$$\partial_{xxxx}\phi = (12a^2 - 40a^3x^2 + 16a^4x^4)\exp[-a(x^2 + y^2 + z^2)], \quad (A1)$$

$$\partial_{xxyy}\phi = -2ay(12a^2x - 8a^3x^3)\exp[-a(x^2 + y^2 + z^2)], \quad (A2)$$

$$\partial_{xyyy}\phi = (4a^2x^2 - 2a)(4a^2y^2 - 2a)\exp[-a(x^2 + y^2 + z^2)], \quad (A3)$$

$$\partial_{xxxz}\phi = -2az(12a^2x - 8a^3x^3)\exp[-a(x^2 + y^2 + z^2)], \quad (A4)$$

$$\partial_{xyyz}\phi = 4a^2yz(4a^2x^2 - 2a)\exp[-a(x^2 + y^2 + z^2)], \quad (A5)$$

$$\partial_{xxzz}\phi = (4a^2x^2 - 2a)(4a^2z^2 - 2a)\exp[-a(x^2 + y^2 + z^2)], \quad (A6)$$

where $\phi = \exp[-a(x^2 + y^2 + z^2)]$.

Other entities can be achieved by cyclic permutation of x, y, z .

Let $\mathbf{M} = \nabla \times \nabla \times \Psi_j$, the entities of \mathbf{M} are shown below:

$$\mathbf{M}_{11} = (\partial_x^2\partial_y^2 + \partial_x^2\partial_z^2 + \partial_z^2\partial_y^2 + \partial_x^4 + \partial_y^4 + \partial_y^2\partial_z^2)\phi_j, \quad (A7)$$

$$\mathbf{M}_{12} = -(\partial_x^3\partial_y + \partial_z^2\partial_x\partial_y + \partial_x\partial_y^3)\phi_j, \quad (A8)$$

$$\mathbf{M}_{13} = -(\partial_x^3\partial_z + \partial_x\partial_z^3 + \partial_x\partial_z\partial_y^2)\phi_j, \quad (A9)$$

$$\mathbf{M}_{22} = (\partial_y^2\partial_x^2 + \partial_x^2\partial_z^2 + \partial_z^2\partial_x^2 + \partial_x^4 + \partial_z^4 + \partial_y^2\partial_z^2)\phi_j, \quad (A10)$$

$$\mathbf{M}_{23} = -(\partial_z\partial_y^3 + \partial_z^3\partial_y + \partial_z\partial_y\partial_x^2)\phi_j, \quad (A11)$$

$$\mathbf{M}_{31} = \mathbf{M}_{13}, \quad (A12)$$

$$\mathbf{M}_{32} = \mathbf{M}_{32}, \quad (A13)$$

$$\mathbf{M}_{33} = (\partial_x^2\partial_y^2 + \partial_y^2\partial_x^2 + \partial_z^2\partial_x^2 + \partial_x^4 + \partial_y^4 + \partial_z^2\partial_y^2)\phi_j. \quad (A14)$$

ACKNOWLEDGMENT

The authors would appreciate the financial support from the National Natural Science Foundation of China under Grant 61427803 and Grant 61761017.

REFERENCES

- [1] V. Cingoski, N. Miyamoto, and H. Yamashita, "Element-free Galerkin method for electromagnetic field computations," *IEEE Trans. Magnetics*, vol. 34, pp. 3236-3239, 1998.
- [2] S. A. Viana and R. C. Mesquita, "Moving least square reproducing kernel method for electromagnetic field computation," *IEEE Trans. Magnetics*, vol. 35, pp. 1372-1375, 1999.
- [3] G. Ala, E. Francomano, A. Tortorici, E. Toscano, and F. Viola, "Smoothed particle electromagnetics: A mesh-free solver for transients," *J. Comput. and Applied Math.*, vol. 191, pp. 194-205, 2006.
- [4] T. Kaufmann, C. Fumeaux, and R. Vahldieck, "The meshless radial point interpolation method for time-domain electromagnetics," *IEEE MTT-S International Microwave Symposium Digest*, pp.

- 61-64, 2008.
- [5] Y. Yu and Z. Chen, "A 3-D radial point interpolation method for meshless time-domain modeling," *IEEE Trans. Microw. Theory Tech.*, vol. 57, pp. 2015-2020, 2009.
- [6] Y. Yu and Z. Chen, "Towards the development of an unconditionally stable time-domain meshless method," *IEEE Trans. Microw. Theory Tech.*, vol. 58, pp. 578-586, 2018.
- [7] B. Jiang, J. Wu, and L. A. Povinelli, "The origin of spurious solutions in computational electromagnetics," *J. Comput. Physics*, vol. 125, pp. 104-123, 1996.
- [8] T. Kaufmann, C. Engstrom, C. Fumeaux, and R. Vahldieck, "Eigenvalue analysis and longtime stability of resonant structures for the meshless radial point interpolation method in time domain," *IEEE Trans. Microw. Theory and Tech.*, vol. 58, pp. 3399-3408, 2010.
- [9] S. Lowitzsch, "Matrix-valued radial basis functions: Stability estimates and applications," *Advances Comput. Math.*, vol. 23, pp. 299-315, 2005.
- [10] S. Lowitzsch, "A density theorem for matrix-valued radial basis functions," *Numerical Algorithms*, vol. 39, pp. 253-256, 2005.
- [11] S. Lowitzsch, "Approximation and Interpolation Employing Divergence-free Radial Basis Functions with Applications," *Ph.D. Dissertation*, Texas A&M University, 2002.
- [12] H. Wendland, "Divergence-free kernel methods for approximating the Stokes problem," *Society for Industrial and Applied Mathematics Journal on Numerical Analysis*, vol. 47, pp. 3158-3179, 2009.
- [13] C. P. McNally, "Divergence-free interpolation of vector fields from point values—exact $\nabla \cdot \mathbf{B} = 0$ in numerical simulations," *Monthly Notices of the Royal Astronomical Society: Letters*, vol. 413, pp. L76-L80, 2011.
- [14] S. Yang, Z. Chen, Y. Yu, and S. Ponomarenko, "A divergence-free meshless method based on the vector basis function for transient electromagnetic analysis," *IEEE Trans. Microw. Theory Tech.*, vol. 62, pp. 1409-1416, 2014.
- [15] J. Zhang, J. Lu, Y. Liu, and S. Yang, "A vector meshless method for transient vector wave equations," *2018 International Appl. Comp. Electro. Society (ACES) Symp.*, Aug. 2018.
- [16] D. Jiao and J. Jin, "A general approach for the stability analysis of the time-domain finite-element method for electromagnetic simulations," *IEEE Trans. Antenna. Propag.*, vol. 50, pp. 1624-1632, 2002.
- [17] D. Smithe, J. Cary, and J. Carlsson, "Divergence preservation in the ADI algorithms for electromagnetics," *J. Comput. Phys.*, vol. 228, pp. 7289-7299, 2009.

- [18] O. Vlasiuk, T. Michaels, N. Flyer, and B. Fornberg, "Fast high-dimensional node generation with variable density," *Computers & Mathematics with Applications*, vol. 76, no. 7, pp. 1739-1757, 2018.



Shunchuan Yang received the B.S., M. S. and Ph.D. degrees from Sichuan University, China, in 2009, Zhejiang University, China, in 2012, and Dalhousie University, Canada, in 2015, respectively. Yang joined Beihang University as an Associate Professor in 2017. His research

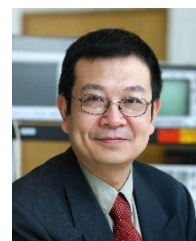
interests include development of advanced numerical methods for computational electromagnetics (CEM) both in time and frequency domains and their applications in integrated circuits modeling, multiphysics and complex media modeling. Yang was a recipient of Killam Awards of Dalhousie University in 2014 and Chinese Government Award for Outstanding Self-financed Students Abroad in 2013.



Donglin Su received the B.S., M.S., and Ph.D. degrees in Electronic Engineering from Beihang University (BUAA), Beijing, China, in 1983, 1986, and 1999, respectively. In 1986, she joined the Faculty of School of Electronics and Information Engineering, BUAA, where

she is currently a Full Professor. Her research interests include the numerical methods for microwave and millimeter-wave integrated circuits and systematic electromagnetic compatibility design of various aircrafts.

She is a senior member of the Chinese Institute of Electronics. She is the General Chair of 2018 International ACES Symposium and the Chair of Beijing Chapter of the IEEE Antennas and Propagation Society and the Deputy Chair of the Antennas Society, Chinese Institute of Electronics.



Zhizhang (David) Chen received the Master degree in Radio Engineering from Southeast University, P. R. China, the Ph.D. degree in Electrical Engineering from the University of Ottawa, Canada. He was a NSERC Post-doctoral Fellow with McGill University, Montreal,

Canada, in 1993. He is currently a Professor with Dalhousie University, Halifax, Nova Scotia, Canada, where he had also served as the Head of the Department of Electrical and Computer Engineering. He has been

an Adjunct or Visiting Professor with the University of Nottingham of UK, École Nationale Supérieure des Télécommunications de Bretagne of France, Shanghai Jiao Tong University, Beijing University of Aeronautics and Astronautics, Fuzhou University, Hong Kong University of Science and Technology and the University of Electronic Science and Technology of China.

Chen has authored and co-authored over 370 journal and conference papers in computational electromagnetics, RF/microwave electronics, antennas, and wireless technologies. He was one of the originators of the unconditionally stable methods that have been highly cited and used. He and his team also developed a number of nonlinear ultra-wideband receivers and planar wireless power transfer transmitting and receiving structures.

He has been an Associate Editor of the recently founded IEEE Journal on Multiscale and Multiphysics

Computational Techniques (2016-2019) and Guest Editors of several professional journals and magazines. He has been invited to give many invited talks and plenary speeches at various international meetings, conferences and forums. He was also involved in organizing in many international workshops and conferences as Chair, Co-Chair, session organizer and committee members. His current research interests are in time-domain electromagnetic modeling techniques, ultra-wideband wireless communication systems and wireless power transfer. He received of the 2005 Nova Scotia Engineering Award, a 2006 Dalhousie graduate teaching award, the 2007 & 2015 Dalhousie Faculty of Engineering Research Award, the 2013 IEEE Canada Fessenden Medal and Dalhousie University Professorship. He is the Fellow of the IEEE, the Canadian Academy of Engineering and the Engineering Institute of Canada.